

The Eclipsing Cataclysmic Variable Lanning 386: Dwarf Nova, SW Sextantis Star, or Both?¹

Steve Brady

sbrady10@verizon.net

AAVSO, 25 Birch Street, Cambridge, MA 02138

John R. Thorstensen

john.thorstensen@dartmouth.edu

Dartmouth College, Department of Physics and Astronomy, 6127 Wilder Lab, Hanover, NH 03755

Michael D. Koppelman

michael@aps.umn.edu

University of Minnesota, Department of Astronomy, 116 Church St. SE, Minneapolis, MN 55455

Jose Luis Prieto

prieto@astronomy.ohio-state.edu

Ohio State University, Department of Astronomy, 140 W. 18th Ave., Columbus, OH 43210

Peter M. Garnavich, Alec Hirschauer, and Michael Florack

pgarnavi@nd.edu; ahirsch1@nd.edu; mflorack@nd.edu

University of Notre Dame, Physics Department, 225 Nieuwland Hall, Notre Dame, IN 46556

ABSTRACT

We present photometry and spectroscopy of the suspected cataclysmic variable (CV) Lanning 386. We confirm that it is a CV, and observe deep eclipses, from which we determine the orbital period P_{orb} to be 0.1640517 ± 0.0000001 d ($= 3.94$ h). Photometric monitoring over two observing seasons shows a very active system with frequent outbursts of variable amplitude, up to ~ 2 mag. The spectrum in quiescence is typical of dwarf novae, but in its high state the system shows strong He II emission and a broad C IV Wolf-Rayet feature. This is unusual for dwarf novae in outburst and indicates a high excitation. In its high state the system shows some features reminiscent of an SW Sextantis-type CV, but lacks others. We discuss the classification of this puzzling object.

Subject headings: Stars

1. Introduction

Cataclysmic variables (CVs) are close binary stars in which a white dwarf primary accretes matter via Roche lobe overflow from a secondary, which usually resembles a lower main-sequence star (Warner 1995). In most CVs an accretion disk encircles the white dwarf. Optical emission can come from several locations in the system. The gas stream from the secondary star strikes the outer rim of the accretion disk producing a rapidly fluctuating bright spot (or hot spot). The accretion disk often dominates the light, and instabilities in the disk can produce large variations in the system brightness. Strong white-dwarf magnetic fields can truncate or even entirely disrupt the accretion disk, allowing material to fall directly onto the white dwarf. In many systems the accumulated hydrogen-rich material can undergo a thermonuclear runaway, creating a classical nova outburst. The range of phenomena seen in CVs means that determining the subclass of any example can require extensive photometric and spectroscopic study.

H. H. Lanning (Lanning 1973 and subsequent papers) conducted a search for ultraviolet-bright (UV) sources in the galactic plane by visually examining plates taken with the Palomar Oschin Schmidt. To date, six supplements have been published, revealing a total of 724 UV sources. Six of these are included in the *Catalog and Atlas of Cataclysmic Variables* (Downes et al. 2001) as confirmed or suspected CVs; they are listed in Table 1.

Eracleous et al. (2002) presented a spectrum of Lanning 386 which showed apparent CV features – a blue continuum, He I absorption lines, and broad Balmer emission lines. The extensive photometric and spectroscopic observations we present here establish that Lanning 386 is indeed a deeply-eclipsing CV with $P_{\text{orb}} = 0.1640517 \pm 0.0000001$ d. Intriguingly, it shares characteristics of both the dwarf novae – CVs that undergo occasional eruptions thought to be caused by a disk instability – and the SW Sextantis stars (Thorstensen et al. 1991), a subclass of the persistently-bright novalike variables.

2. Observations

2.1. Photometry

We began routine monitoring of Lanning 386 on 2005 June 25, with a 0.25 m robotic survey telescope at the lead author’s private observatory in southern New Hampshire. The system was

¹Dedicated to Howard Lanning, who died in 2007 December.

programmed to automatically monitor a list of poorly-studied CV candidates and to initiate time series photometry if and when an outburst was detected. The first outburst of Lanning 386 was detected 2005 September 12 UT, after eleven weeks of monitoring. Time series observations (detailed in Table 3) began immediately, and revealed two eclipses separated by ~ 3.9 hr, about 1.5 mag deep. Thereafter, time series observations were obtained every clear night for 5 months in 2005 and another 5 months in 2006, yielding over 3,000 photometric observations. A 0.4 m telescope at the same observatory was used along with the 0.25 m, and all observations were unfiltered due to the star’s faintness. Integration times were 300 sec with the 0.25 m telescope and 180 sec with the 0.4 m. All images were bias subtracted and flat-field corrected. Ensemble photometry was performed using 12 relatively isolated comparison stars. We established a rough zero point using V magnitudes of four of these stars (Figure 1) measured with the MDM 2.4m telescope (see below); Table 2 gives their positions and magnitudes. The mean scatter of the differential photometry was ~ 1 percent. The unfiltered photometry has a significant color term, and the zero points of the two filter photometry sessions described below were slightly discrepant, so we estimate the uncertainty in the photometric zero point to be ± 0.1 mag.

Our filter photometry is from the 2.4 m Hiltner telescope at MDM Observatory on Kitt Peak. A 2048^2 SITe CCD detector, cropped to 1024^2 to minimize read time, gave a 4.7 arcmin square field of view. We obtained single sets of short (60 - 120 s) exposures through $UBVI$ filters on 2005 September 15 and 2007 June 24 UT, measured them using the IRAF⁰ implementation of DAOPHOT (Stetson 1987), and derived transformations to the Johnson/Cousins photometric system using observations of Landolt (1992) standard-star fields. The zero points for the two sets of observations differed by ~ 0.06 mag in V . The 2005 September 15 observations show Lanning 386 at $V = 15.20$, $B - V = +0.08$, $U - B = -0.63$, and $V - I = +0.29$, while the 2007 June 24 observation yields $V = 17.28$, $B - V = +0.27$, $U - B = -0.87$, and $V - I = +1.07$.

2.2. Spectroscopy

Our spectra come from three different instruments on two different telescopes, as listed in Table 4.

Our most extensive spectroscopy is from the Hiltner telescope, equipped with the MDM Modular spectrograph, a 600 line mm^{-1} grating, and the same 2048^2 SITe detector used for the filter photometry. The Modspec observations were taken by one of us (JRT) without awareness that eclipses had been discovered, and were therefore aimed largely at determining P_{orb} . The spectra cover from 4200 to 7500 Å, with 2 Å pixel^{-1} sampling and ~ 3.5 Å resolution (FWHM). The observing and reduction procedures were as described in Sheets et al. (2007).

⁰IRAF is distributed by the National Optical Astronomy Observatory, which is operated by the Association of Universities for Research in Astronomy, Inc., under cooperative agreement with the National Science Foundation.

We also obtained time-series spectra of Lanning 386 in its bright state using the Kitt Peak National Observatory (KPNO) Mayall 4 m telescope and RC spectrograph. The T2KB CCD detector, KPC10a grating, and a 1 arcsec slit provided an average dispersion of $2.8 \text{ \AA pixel}^{-1}$ and a useful range between 3700 and 8000 \AA , with some order overlap beyond 7400 \AA . The slit was rotated to the parallactic angle to prevent differential slit losses. The spectra were bias subtracted, flat-field corrected using images of an internal quartz lamp, extracted using the IRAF *twodspec* package, and wavelength calibrated against HeNeAr lamp exposures taken from time to time as the telescope tracked. We applied a flux calibration derived from observations of the spectrophotometric standard BD +28° 4211.

Finally, we have two 600-s exposures of Lanning 386 taken during twilight on 2006 Dec 8 UT, using the MDM Hiltner telescope and OSU Boller and Chivens CCD spectrograph (CCDS). The spectra were reduced in the same way as the KPNO data described above. The 5000-6000 \AA continuum is ~ 2.4 mag fainter than in the KPNO spectra, confirming that the system was in quiescence.

3. Analysis

3.1. Ephemeris

Table 5 lists the observed times of mid-eclipse. These yield a unique ephemeris,

$$\text{Minimum light} = \text{Heliocentric JD } 2453625.5867(4) + 0.1640517(1)E, \quad (1)$$

where E is an integer and the parentheses give uncertainties in the last digits. Radial velocities of the $\text{H}\alpha$ emission line (discussed below) give essentially the same period, namely 0.1640530(11) d, without ambiguity caused by uncertainty in the number of cycles elapsed between observing runs. All phases in this paper refer to the eclipse ephemeris.

3.2. Light Curve and Long-Term Variations

In Figures 2 and 3 we show representative light curves in quiescence and outburst, constructed by folding two consecutive observation sessions using the ephemeris (Eqn. 1). The quiescent plot, from observations made between 2005 September 27 and October 1 UT, shows a pre-eclipse hump; this feature usually arises from the “hot spot” where gas streaming from the secondary star strikes the disk. The hot spot contribution is not evident in the outburst plot, made from observations taken 2006 July 16 and 17 UT. The eclipse depth is roughly the same in each state.

Figure 4 shows all the photometry folded on the ephemeris and makes evident the long term variations in the mean magnitude. The histogram of the median magnitude for each of the dates in Table 3, shown in Figure 5, suggests an quiescent state near $m = 17.2$ (with some variability),

an intermediate stage at $m = 15.9$ and an outburst state at $m = 15.3$. This range of brightness is also evident from visual inspection of Figure 4. Figure 6 shows a typical portion of the long-term light curve, from the 2006 observing season.

3.3. Spectral Appearance and Analysis

The top trace of Fig. 7 shows the mean of the low-state Modspec spectra. The mean spectrum is typical of dwarf novae at minimum light; Table 6 gives identifications and measurements of the emission features. The synthetic magnitude is $V = 17.5$, using the passband given by Bessell (1990), which is roughly consistent with the low state photometry outside of eclipse. At the red end, the absorption bands of an M dwarf are visible. We estimated the spectral class and flux contribution of the M dwarf by subtracting scaled M-dwarf library spectra from the low-state spectrum and judging how well the M-dwarf features were accounted for; this yielded a spectral type $M3.3 \pm 0.8$ and a contribution to the total light corresponding to $V = 20.3 \pm 0.6$ (including estimated calibration uncertainty). Using (1) the measured P_{orb} , (2) the condition that the secondary fill the Roche lobe, and (3) a broad range of plausible secondary star masses M_2 (from 0.2 to 0.5 M_{\odot} ; Baraffe & Kolb 2000), we estimate that the secondary’s scaled M-dwarf library spectra from the low-state spectrum and judging how well the M-dwarf features were accounted for; this yielded a spectral type $M3.3 \pm 0.8$ and a contribution to the total light corresponding to $V = 20.3 \pm 0.6$ (including estimated calibration uncertainty). Using (1) the measured P_{orb} , (2) the condition that the secondary fill the Roche lobe, and (3) a broad range of plausible secondary star masses M_2 (from 0.2 to 0.5 M_{\odot} ; Baraffe & Kolb 2000), we estimate that the secondary’s radius $R_2 = 0.4 \pm 0.07 R_{\odot}$ – fortunately, R_2 at a fixed P_{orb} depends only weakly on M_2 , roughly as $M_2^{1/3}$. Finally, using the calibration of the relation between spectral type and V -band surface brightness given by Beuermann (2006), we estimate $M_V = 11.1 \pm 1.0$ for the secondary, giving an apparent distance modulus $m - M = 9.1 \pm 1.2$. At Galactic latitude $b = -5.8$ there is likely to be substantial dust extinction; Schlegel et al. (1998) estimate that extragalactic objects in this direction undergo reddening $E(B - V) = 0.54$. The actual reddening appears to be considerably less than this upper limit; most dwarf novae in outburst have $B - V = 0$, within ± 0.1 mag or so (Bruch & Engel 1994), so our outburst color suggests $E(B - V) < 0.2$ or so. If so, the nominal distance would be ~ 500 pc.

The bright state KPNO spectra cover both eclipse and out-of-eclipse phases. As shown in Figure 8, the average spectrum in the bright state shows broad Balmer emission lines on a continuum that is considerably bluer than in the low state. Several He I emission lines such as $\lambda\lambda 6678, 5876, 5016, 4922$ are clearly seen, but the strongest non-hydrogen feature is the bright He II $\lambda 4686$ line, which is blended with the C III/N III Bowen complex. He II is so prominent in this star that the usually weak line at $\lambda 5412$ is also easily detected. A broad feature in the spectrum at $\lambda 5806$ is evidently a C IV feature which is common in Wolf-Rayet stars, but unusual in cataclysmic variables. Schmidtobreick (2003) found the line in the old nova V840 Oph and suggested the star had a carbon over-abundance. However, Groot et al. (2000) identified C IV in SW Sex and

attributed it to a particularly high-excitation state for the star. In eclipse, the continuum remains blue, but its slope is greatly reduced. Between 6000 Å and 4000 Å the continuum rises by a factor of 2.9 (in f_λ) out of eclipse but only by a factor of 1.6 in eclipse. However, in eclipse the He II emission remains one of the strongest lines in the spectrum. The ratio of fluxes between He II $\lambda 4686$ and H β is 1.2 out of eclipse and 0.64 during eclipse.

If Lanning 386 is a dwarf nova, its high-state spectrum is unusual; we comment on this more extensively in the Discussion.

Figure 9 shows phase-resolved greyscale representations of our high- and low-state spectra. To construct these, the spectra were first divided by the continuum and cleaned of residual cosmic rays; then for each orbital phase we averaged spectra whose phases were close to the target phase, using a Gaussian in phase for the weighting function. Finally, all the spectra were stacked together to form a two-dimensional image, with a second cycle repeated for continuity. We created separate images from the high-state KPNO data and the low-state MDM Modspec data.

Examination of Fig. 9 shows a host of interesting differences between the two states. In the low state (top two panels), the emission lines have two approximately equal peaks, while in the high state (lower two panels) show more complex behavior; in particular, phase-dependent absorption is seen in He I $\lambda\lambda 4921$, 5015, and 5876, and in the metal feature near $\lambda 5175$. In H β (and in H α , which is not shown here) there is a sharp component that moves approximately in antiphase to the bulk of the line. The phasing of the sharp component’s motion is approximately as expected for emission from the heated face of the secondary. The high-state image has good coverage across the eclipse at phase $\phi = 0$; because the emission lines are eclipsed less strongly than the continuum, the continuum division used in this representation causes an increase in the apparent emission strength. This is artificial, but the sharp red-to-blue swing in the line’s central wavelength is evidently real (see below).

4. Radial Velocities

We measured radial velocities of the H α emission in the Modspec and KPNO spectra using a convolution algorithm described by Schneider & Young (1980) and Shafter (1983). For the low-state Modspec data the convolving function consisted of positive and negative Gaussians with a full-width at half maximum (FWHM) of 550 km s $^{-1}$, separated by 1920 km s $^{-1}$, which emphasized the steep sides of the line profile. The corresponding figures for the slightly narrower line profile in the high-state data were respectively 365 and 1645 km s $^{-1}$.

We searched the velocity time series for periods; this exercise independently reproduced the same period found in the eclipses, with no cycle-count ambiguity on any time scale. Remarkably, the high- and low-state velocities agreed very well in phase, amplitude, and zero point, despite differences in instrumentation as well as photometric state. The modulation is accurately sinusoidal, *except* for a rapid swing redward and then blueward across the eclipse – the classic signature of the

eclipse of a rapidly-rotating object. Excluding the velocities affected by the rotational disturbance, holding P fixed at 0.1640517 d, and fitting a sinusoid of the form $v(t) = \gamma + K \sin[2\pi(t - T_0)/P]$ yields

$$T_0 = \text{HJD } 2453980.6815 \pm 0.0010, \quad (2)$$

$$K = 152 \pm 5 \text{ km s}^{-1}, \quad (3)$$

$$\gamma = -51 \pm 4 \text{ km s}^{-1}, \text{ and} \quad (4)$$

$$\sigma = 18 \text{ km s}^{-1}, \quad (5)$$

where σ is the RMS scatter about the best fit. Fig. 10 shows the velocities folded on the eclipse ephemeris.

The sinusoid fitted to the velocities is defined so that T_0 is the time at which $v(t)$ crosses the system velocity γ from blue to red. If the emission lines trace the motion of the white dwarf, this must occur opposite the eclipse, at phase $\phi = 0.5$. The fitted T_0 corresponds to $\phi = 0.530 \pm 0.006$, or a phase lag of $11^\circ \pm 2^\circ$ compared to this expectation. This suggests that the emission line velocities do not trace the white dwarf motion precisely.

5. Discussion

Our photometry shows Lanning 386 to be an active, eclipsing CV, with $P_{\text{orb}} = 3.94$ h and an eclipse depth of ~ 1.5 mag. Monitoring over many months shows bright outbursts reaching $V \approx 15.2$ from a quiescent state with $V \approx 17.2$.

Lanning 386 does not fit neatly into any CV subclass. The long-term variability resembles that of a dwarf nova, and at minimum light the spectrum is typical of that class. However, when most dwarf novae outburst, their Balmer emission becomes very weak, and broad absorption wings appear (e.g., Thorstensen et al. 1998); it is also unusual (though not unknown) for He II to become prominent (e.g., Hessman et al. 1984). The high-state spectrum seen here is very much unlike this, resembling instead that of a novalike variable. The He I line profiles, and the unusual strength of He II, are reminiscent of an SW Sextantis star (Thorstensen et al. 1991). In addition, Lanning 386 is similar to other SW Sex stars in that the emission lines are eclipsed much more shallowly than the continuum, indicating a spatially extended source. The rotational disturbance around eclipse is also seen in some other SW Sex stars (e.g., Rodríguez-Gil et al. 2004). However, other canonical SW Sex characteristics are missing here. The emission line radial-velocity phase in SW Sex stars lags far behind (by $> 45^\circ$) the phase expected for the white dwarf motion, based on the eclipse ephemeris, but in Lanning 386 the phase lag is only $\sim 11^\circ \pm 2^\circ$. In addition, while the He I lines do appear in absorption for part of the orbit, in other SW Sex stars the absorption appears near phase 0.5, whereas it appears somewhat later here.

Nonetheless, the unusual maximum-light spectrum suggests that we should consider carefully whether the long-term light curve in Fig. 6 forces us to classify this star as a dwarf nova. Might

another mechanism explain the variability in a manner more consistent with the maximum-light spectrum?

Many novalike variables, and many SW Sex stars in particular, are also VY Scl stars – novalike variables that occasionally fade deeply for varying amounts of time, for reasons that are not entirely understood. Might Lanning 386 be a VY Scl star masquerading as a dwarf nova? This seems unlikely, for two reasons. First, the long-term light curves of VY Scl stars tend to look quite different from those of dwarf novae – VY Scl stars typically remain in a high state for months or years, and only occasionally fade by large amounts, up to 5 mag (see examples in Honeycutt & Kafka 2004). The light curve here, by contrast, consists of frequent, moderate-amplitude outbursts from a faint state. Second, the spectra of VY Scl stars in their faint states look as if accretion has nearly stopped, with the Balmer emission lines typically becoming very narrow and the underlying stars becoming evident (Shafter et al. 1983; Schneider et al. 1981). This is very different from the essentially normal dwarf nova spectrum seen here.

The DQ Her stars, also called intermediate polars, are magnetic systems (for a review, see Patterson 1994); some of these undergo outbursts that at least superficially resemble dwarf nova outbursts. Typically, DQ Her outbursts are infrequent compared to those of most dwarf novae; they also tend to decay rapidly (Hellier et al. 1997). For this reason, there is little spectroscopy available for outbursts of these systems. However, spectra do exist for EX Hya in outburst, which, show strong emission lines with interesting velocity structure, reminiscent of the SW Sex stars (Hellier et al. 1989, 2000). In this way, EX Hya resembles Lanning 386, but the morphological fit is imperfect – the brightenings we see in Lanning 386 appear to be more frequent than those seen in most DQ Her stars. Also, we have (as of yet) no direct evidence that Lanning 386 is a magnetic system, because we are unaware of any searches for the coherent pulsations and/or circular polarization that would prove the case.

It has been suggested that the outbursts seen in some magnetic systems are due to mass-transfer bursts rather than the disk instabilities that are thought to cause normal dwarf nova outbursts². During a period of increased mass transfer, material overflowing the disk could give rise to enhanced emission – there is evidence for this in EX Hya (Hellier et al. 2000). It may be that the outbursts seen in Lanning 386, whatever their trigger, involve enhanced mass transfer – which may or may not be exclusive to magnetic systems.

We can summarize the morphological conundrum presented by Lanning 386 as follows: Its minimum-light spectrum and the light curve suggest it is a dwarf nova with frequent, relatively low-amplitude outbursts, while at maximum light it resembles a novalike variable, with some (but not all) the characteristics of an SW Sex star. EX Hya, a magnetic system, shows a similar set of symptoms, but the presentation is not identical.

²It is possible that mass-transfer bursts could be triggered by an event in the disk.

6. Acknowledgments

While this paper was in production we learned that H. Lanning had died in 2007 December; we thank him posthumously for encouraging us to get spectra of this star and dedicate this paper to his memory. JRT acknowledges support from the National Science Foundation through awards AST-0307413 and AST-0708810. We thank the KPNO and MDM staffs for their conscientious support, and the Tohono O’odham Nation for letting us use their mountain for a while to explore the universe we all share. Finally, we thank the referee for a careful reading and numerous helpful suggestions.

REFERENCES

- Baraffe, I., & Kolb, U. 2000, MNRAS, 318, 354
- Bessell, M. S. 1990, PASP, 102, 1181
- Beuermann, K. 2006, A&A, 460, 78
- Bruch, A., & Engel, A. 1994, A&AS, 104, 79
- Downes, G. et al. 2001, PASP, 113, 764
- Eracleous, M. et al. 2002, PASP, 114, 207E
- Groot, P. J., Rutten, R. G. M., and van Paradijs, J. 2000, New Astro. Rev., 44, 137
- Hellier, C., Kemp, J., Naylor, T., Bateson, F. M., Jones, A., Overbeek, D., Stubbings, R., & Mukai, K. 2000, MNRAS, 313, 703
- Hellier, C., Mason, . O., Smale, A. P., Corbet, R. H. D., O’Donoghue, D., Barrett, P. E., & Warner, B. 1989, MNRAS, 238, 1107
- Hellier, C., Mukai, K., & Beardmore, A. P. 1997, MNRAS, 292, 397
- Hessman, F. V., Robinson, E. L., Nather, R. E., & Zhang, E.-H. 1984, ApJ, 286, 747
- Honeycutt, R. K., & Kafka, S. 2004, AJ, 128, 1279
- Horne, K., Lanning, H.H., and Gomer, R.H. 1982, Ap. J. 252, 681
- Landolt, A. U. 1992, AJ, 104, 340
- Lanning, H.H. 1973, PASP, 85 70
- Lanning, H.H. and Meakes, M. 1998, PASP, 110, 586
- Lanning, H.H. and Meakes, M. 2000, PASP, 112, 251

- Liu, W., & Hu, J. Y. 2000, *ApJS*, 128, 387
- Patterson, J. 1994, *PASP*, 106, 209
- Rodríguez-Gil, P., Gänsicke, B. T., Barwig, H., Hagen, H.-J., & Engels, D. 2004, *A&A*, 424, 647
- Schlegel, D. J., Finkbeiner, D. P., & Davis, M. 1998, *ApJ*, 500, 525
- Schmidtobreick, L., Tappert, C., Bianchini, A., and Mennickent, R. E. 2003, *A&A*, 410, 943
- Schneider, D. P. & Young, P. 1980, *ApJ*, 238, 946
- Schneider, D. P., Young, P., & Shectman, S. A. 1981, *ApJ*, 245, 644
- Shafter, A. W. 1983, *ApJ*, 267, 222
- Shafter A.W., Lanning, H.H., Ulrich R.K 1983, *PASP*, 95, 206
- Sheets, H. A., Thorstensen, J. R., Peters, C. J., Kapusta, A. B., & Taylor, C. J. 2007, *PASP*, 119, 494
- Stetson, P. B. 1987, *PASP*, 99, 191
- Thorstensen, J.R., Ringwald, F. A., Wade, R. A., Schmidt, G.D., and Norsworthy, J.E. 1991, *AJ*, 102, 272
- Thorstensen, J. R., Taylor, C. J., & Kemp, J. 1998, *PASP*, 110, 1405
- Warner, B. 1995, *Cambridge Astrophysics Series*, Cambridge, New York: Cambridge University Press, —c1995
- Zacharias, N., Urban, S. E., Zacharias, M. I., Wycoff, G. L., Hall, D. M., Monet, D. G., &

Table 1. Known or Suspected Lanning CVs

Object	Classification	Source
Lanning 10	nl/ux	Horne et al. (1982)
Lanning 17	n:	Lanning (1973)
Lanning 90	ux	Shafter et al. (1983)
Lanning 159 ^a	nl:	Eracleous et al. (2002)
Lanning 302	n:	Lanning & Meakes (1998)
Lanning 386	CV:	Eracleous et al. (2002)
Lanning 420	n:	Lanning & Meakes (2000)

^aLiu & Hu (2000) obtained a spectrum of Lanning 159 that did not support a CV classification; one of us (JRT) also obtained a spectrum with the MDM 2.4 m, using the same MDM modspeg setup described in this paper, which at low signal-to-noise shows H α in absorption with a profile resembling a DA white dwarf.

Table 2. Comparison Stars for Lanning 386

Star	α_{2000} ^a [hh:mm:ss]	δ_{2000} [°:':"]	V
A	21:08:29.82	39:04:43.7	14.633
B	21:08:31.94	39:04:47.1	15.759
C	21:08:32.53	39:05:44.0	16.983
D	21:08:40.15	39:05:06.6	15.976

^aCelestial coordinates are measured from MDM 2.4m images, using a coordinate solution based on numerous UCAC2 stars (Zacharias et al. 2004).

Table 3. Log of Photometric Observations

UT Date	Duration(hr)	Avg mag outside eclipse	Eclipse depth	Comments
2005 Sep 12	5.8	15.4	1.4	Large amplitude outburst
2005 Sep 13	5.2	15.4	1.4	Large amplitude outburst
2005 Sep 14	6.6	15.5	1.5	Large amplitude outburst, Small hump??
2005 Sep 22	6.6	17.3	1.2	Quiet, Strong 0.3 mag hump
2005 Sep 24	6.0	17.3	1.4	Quiet, Strong 0.4 mag hump
2005 Sep 25	6.6	17.4	1.2	Quiet, Strong 0.4 mag hump
2005 Sep 28	6.5	17.4	1.5	Quiet, Small 0.3 mag hump
2005 Oct 02	6.4	17.5	1.3	Quiet, Strong 0.4 mag hump
2005 Nov 03	3.9	16.1	2.0	Minor outburst
2005 Nov 08	3.7	17.4	1.6	Quiet
2005 Nov 13	4.1	16.3	1.6	Minor outburst, 0.3 mag hump
2006 Jul 10	5.8	16.9	2.0	Quiet
2006 Jul 17	6.0	15.2	1.4	Major outburst
2006 Jul 18	5.8	15.2	1.6	Major outburst
2006 Jul 20	6.4	15.5	1.7	Major outburst, fading
2006 Jul 24	5.7	17.0	2.1	Quiet
2006 Aug 09	4.6	16.0	2.3	Minor outburst
2006 Aug 10	7.4	16.2	2.0	Minor outburst
2006 Aug 31	2.2	17.2	1.8	Quiet
2006 Sep 01	5.8	17.2	1.2	Quiet, 0.4 mag hump
2006 Sep 09	6.9	16.8	1.6	Minor flare up or fading
2006 Sep 12	7.3	17.4	1.5	Quiet, 0.3 mag hump
2006 Sep 13	6.7	17.3	1.5	Quiet, 0.3 mag hump
2006 Sep 21	6.4	15.9	2.0	Minor outburst
2006 Sep 22	6.4	16.3	1.9	Minor outburst, fading
2006 Sep 25	6.7	17.5	1.3	Quiet, Strong 0.5 mag hump
2006 Sep 27	4.3	17.4	1.4	Quiet, 0.3 mag hump
2006 Sep 30	6.0	16.2	2.1	Minor outburst
2006 Oct 03	6.6	16.8	1.9	Minor outburst/ fading
2006 Oct 09	5.8	17.5	1.4	Quiet, Strong 0.4 mag hump
2006 Oct 13	3.9	17.5	1.4	Quiet, 0.3 mag hump
2006 Oct 22	6.0	17.7	1.0	Quiet, 0.3 mag hump
2006 Nov 18	3.5	15.1	2.2	Large amplitude outburst
2006 Nov 21	4.8	15.2	1.5	Large amplitude outburst
2006 Nov 24	5.2	15.6	1.8	Large amplitude outburst, fading
2006 Dec 03	4.3	17.2	1.4	Quiet, 0.3 mag hump
2006 Dec 08	3.4	17.2	1.5	Quiet
2006 Dec 09	3.0	17.2	1.5	Quiet
2006 Dec 10	4.1	17.2	1.5	Quiet, 0.3 mag hump
2006 Dec 11	3.1	17.2	1.5	Quiet, 0.3 mag hump
2006 Dec 17	2.4	16.0	1.8	Minor outburst
2006 Dec 19	2.6	17.3	1.4	Quiet
2006 Dec 20	2.0	17.2	1.4	Quiet, 0.2 mag hump
2006 Dec 21	2.0	17.2	1.4	Quiet
2006 Dec 25	2.8	17.1	1.6	Quiet

Table 4. Journal of Spectroscopic Observations

Date (UT)	N	HA start [hh:mm]	HA end [hh:mm]	Instrument ^a	state
2005 Jul 01	2	−0:15	−0:04	mod	low
2005 Sep 09	5	+1:42	+2:27	mod	high
2006 Aug 31	5	−0:17	+4:35	mod	low
2006 Sep 01	11	−1:15	+5:58	mod	low
2006 Sep 02	7	−2:57	−0:38	mod	low
2006 Nov 18	25	+1:28	+4:20	RC	high
2006 Dec 08	2	+1:55	+2:07	CCDS	low
2007 Mar 30	2	−4:01	−3:50	mod	low
2007 Apr 01	2	−4:00	−3:49	mod	low

^amod = MDM 2.4m Hiltner + modspec; RC = KPNO 4m Hiltner + RC spectrograph; CCDS = MDM 2.4m Hiltner + CCDS

Table 5. Observed Eclipses of Lanning 386

HJD(+2,450,000)	Epoch	O-C (sec)	UT Date
3625.58669 ± 0.00044	0	0	2005 Sep 12
3625.75074 ± 0.00091	1	27	2005 Sep 12
3626.73505 ± 0.00041	7	59	2005 Sep 13
3627.55531 ± 0.00002	12	53	2005 Sep 14
3627.71936 ± 0.00044	13	40	2005 Sep 14
3635.59385 ± 0.00049	61	42	2005 Sep 22
3635.75790 ± 0.00156	62	31	2005 Sep 22
3637.56247 ± 0.00002	73	135	2005 Sep 24
3637.72652 ± 0.00002	74	77	2005 Sep 25
3641.66376 ± 0.00067	98	80	2005 Sep 28
3645.60100 ± 0.00002	122	15	2005 Oct 02
3677.59108 ± 0.00058	317	39	2005 Nov 03
3682.51263 ± 0.00002	347	77	2005 Nov 08
3687.59823 ± 0.00002	378	63	2005 Nov 13
3933.67578 ± 0.00002	1878	53	2006 Jul 17
3934.66010 ± 0.00002	1884	53	2006 Jul 18
3934.82415 ± 0.00021	1885	22	2006 Jul 18
3936.62872 ± 0.00002	1896	27	2006 Jul 20
3936.79277 ± 0.00002	1897	21	2006 Jul 20
3940.73001 ± 0.00352	1921	104	2006 Jul 24
3956.80707 ± 0.00159	2019	44	2006 Aug 09
3957.62733 ± 0.00098	2024	20	2006 Aug 10
3957.79138 ± 0.00056	2025	26	2006 Aug 10
3979.77431 ± 0.00067	2159	22	2006 Sep 01
3987.64879 ± 0.0012	2207	-30	2006 Sep 09
3990.60172 ± 0.00002	2225	20	2006 Sep 12
3991.58603 ± 0.00517	2231	-30	2006 Sep 113
3991.75009 ± 0.00076	2232	39	2006 Sep 13
3999.62457 ± 0.00048	2780	302	2006 Sep 21
4000.60888 ± 0.00145	2286	18	2006 Sep 22
4003.56181 ± 0.0016	2304	36	2006 Sep 25
4003.72586 ± 0.00145	2305	40	2006 Sep 25
4005.53043 ± 0.00074	2316	79	2006 Sep 27
4005.69448 ± 0.00123	2317	53	2006 Sep 27
4008.64741 ± 0.00076	2335	36	2006 Sep 30
4011.60034 ± 0.00087	2353	35	2006 Oct 03
4017.50620 ± 0.00058	2389	46	2006 Oct 09
4017.67026 ± 0.00102	2390	44	2006 Oct 09
4022.59181 ± 0.0009	2420	48	2006 Oct 13
4030.63034 ± 0.0018	2469	-37	2006 Oct 22
4057.53482 ± 0.00156	2633	-3	2006 Nov 18
4064.58904 ± 0.00035	2676	30	2006 Nov 24
4072.46352 ± 0.00083	2724	72	2006 Dec 03
4078.53344 ± 0.0012	2761	60	2006 Dec 09
4079.51775 ± 0.00096	2767	29	2006 Dec 10
4089.52490 ± 0.002	2828	64	2006 Dec 20
4090.50921 ± 0.00107	2834	10	2006 Dec 21
4091.49352 ± 0.00091	2840	115	2006 Dec 21
4094.44645 ± 0.00077	2858	60	2006 Dec 24

Table 6. Emission Lines in Quiescence

Feature	E.W. ^a (Å)	Flux (10^{-16} erg cm ⁻² s ¹)	FWHM ^b (Å)
H γ	27	166	28
HeI λ 4471	6	31	36
H β	46	196	30
HeI λ 4921 ^c	8	32	36
HeI λ 5015 ^c	7	32	46
FeII λ 5169	4	17	38
HeI λ 5876	10	39	26
H α	65	227	32
HeI λ 6678	6	20	33
HeI λ 7067	6	20	37

^aEmission equivalent widths are counted as positive.

^bFrom Gaussian fits.

^cThe λ 4921 and 5015 features are generally ascribed to HeI, but may include a contribution from Fe II $\lambda\lambda$ 4924 and 5018.

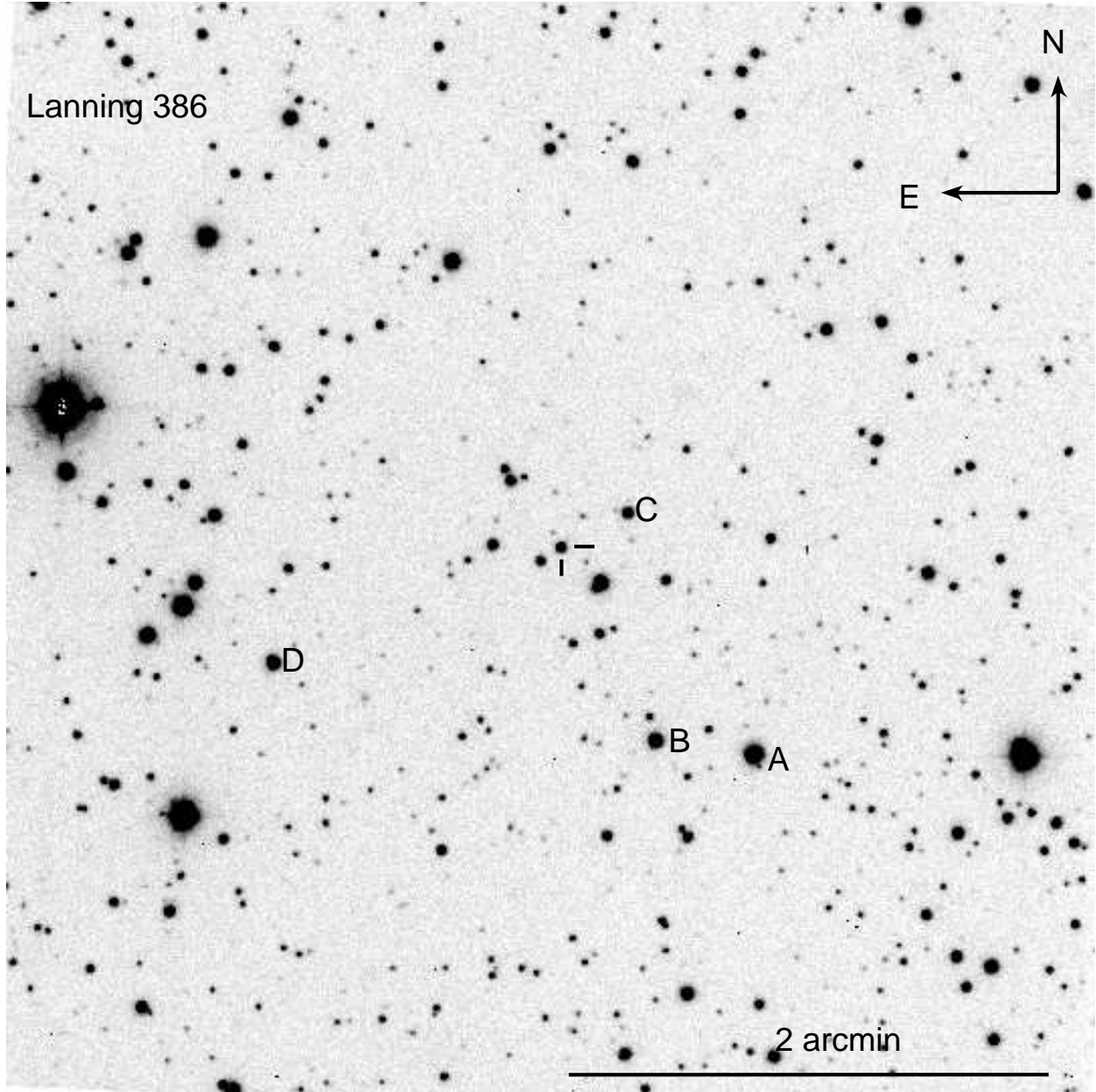


Fig. 1.— A 60-second *V*-band image of Lanning 386 taken with the 2.4m MDM Hiltner telescope, 2007 June 24.93 UT, with Lanning 386 in quiescence. The scale and orientation are as indicated. A coordinate solution for this image based on numerous UCAC-2 stars (Zacharias et al. 2004) puts Lanning 386 at $\alpha = 21^{\text{h}}08^{\text{m}}33^{\text{s}}.97, +39^{\circ}05'35''.3$, referred to the ICRS (equinox 2000).

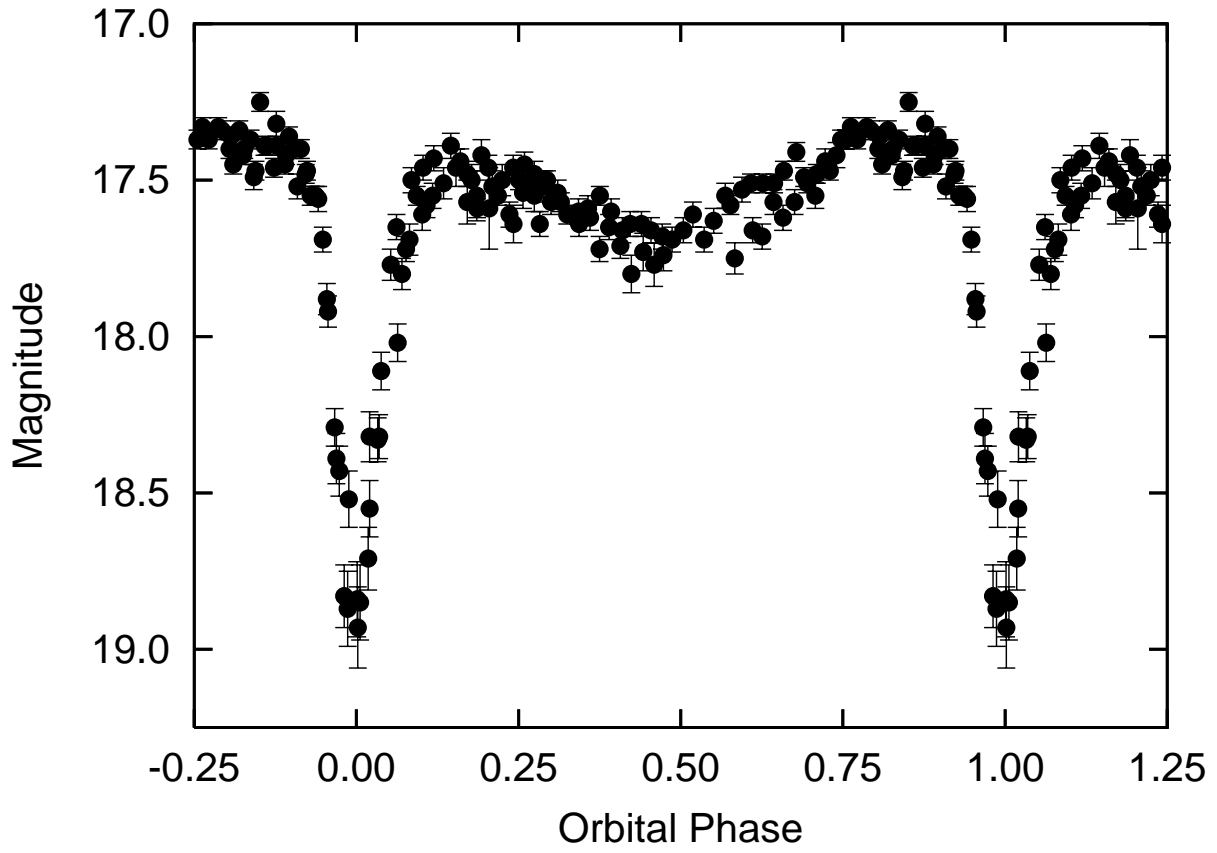


Fig. 2.— Two nights of quiescent-state photometry folded on the orbital period. Note the prominent pre-eclipse hump. The observations are unfiltered, but calibrated to the Johnson *V*-band.

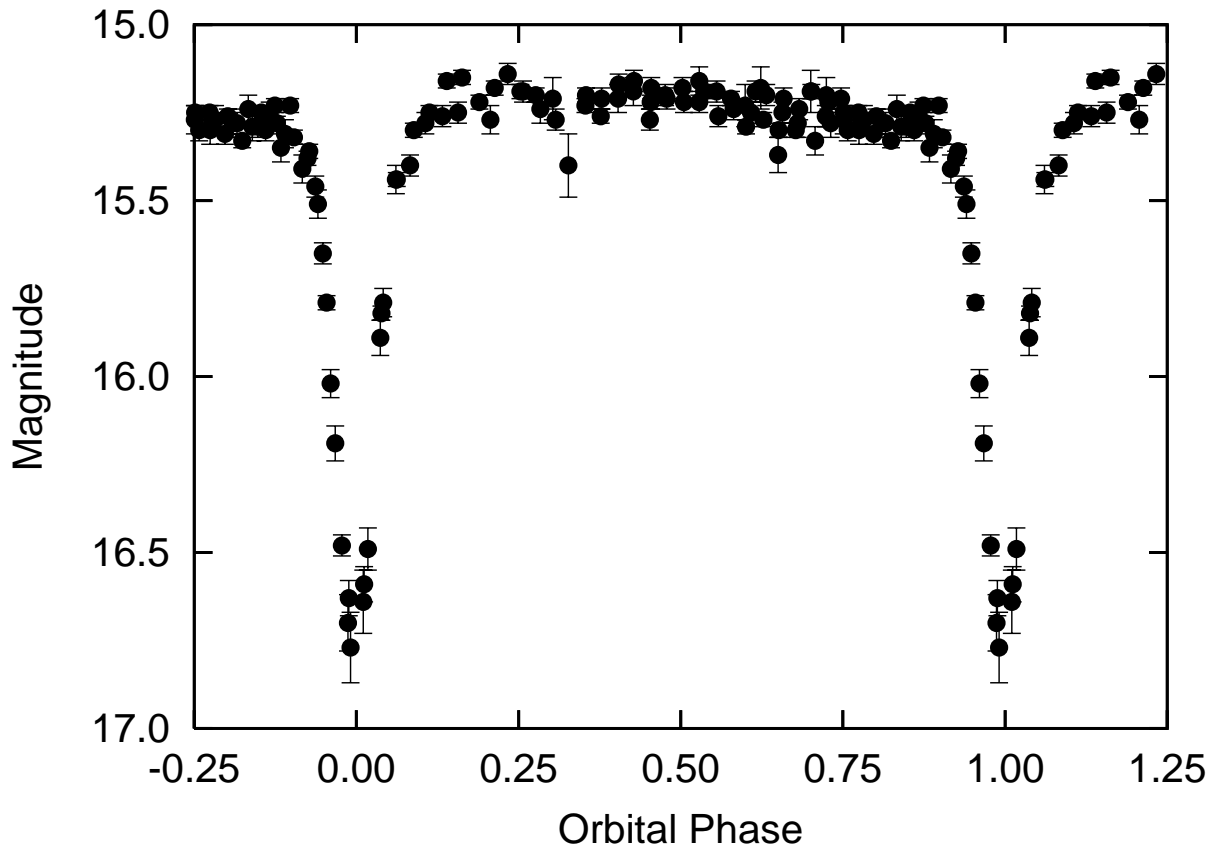


Fig. 3.— Two nights in outburst folded on the orbital period. The observations are unfiltered, but calibrated to the Johnson V -band.

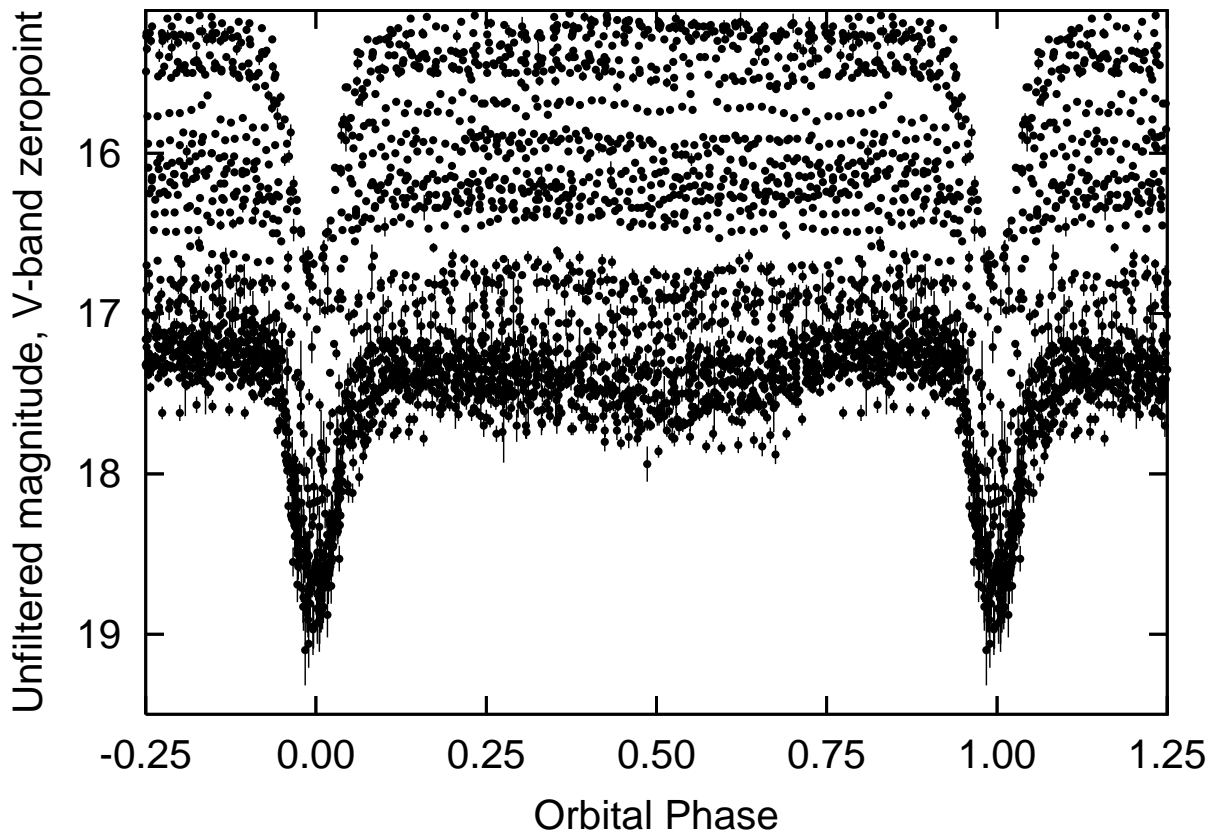


Fig. 4.— All photometric observations folded on the orbital period. Note how the eclipse depth does not vary significantly with brightness. Lanning 386 could be found at nearly any brightness between $V = 17.4$ and 15.2 in 2005-2006.

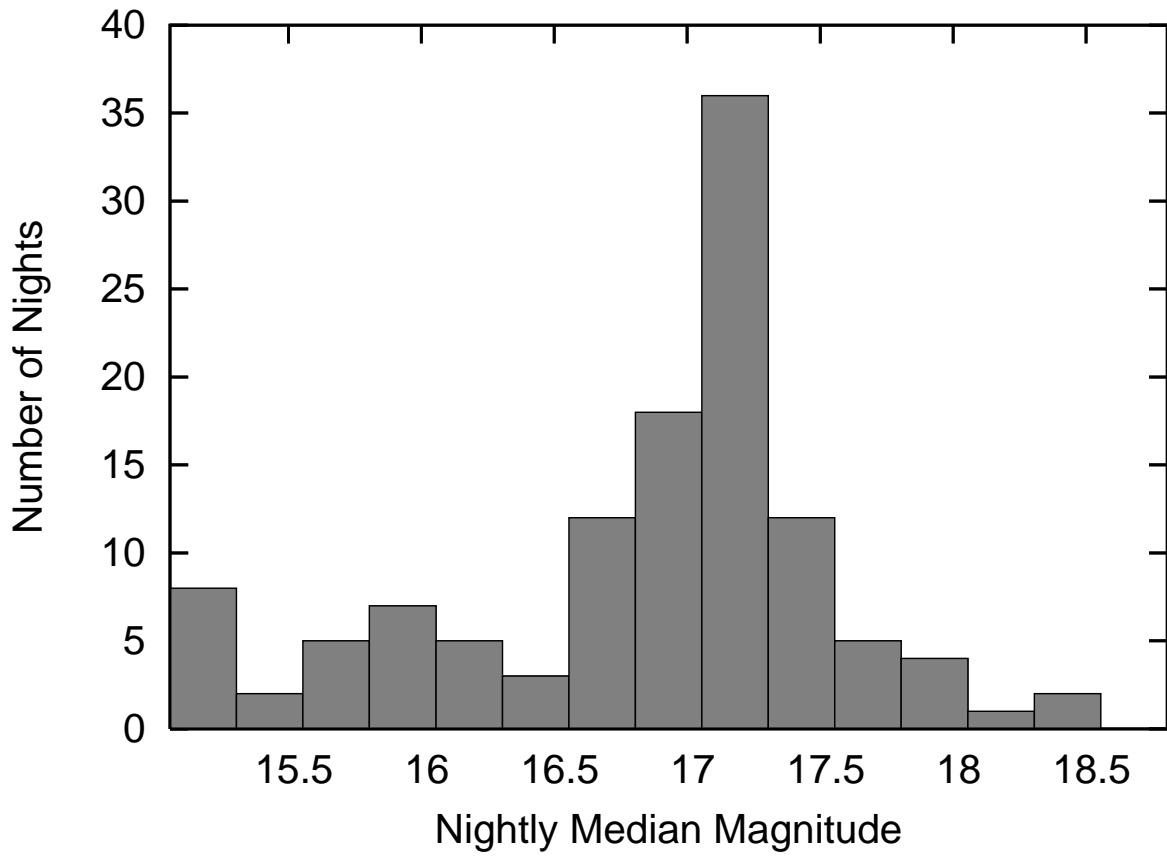


Fig. 5.— Histogram of the median magnitude for each date with observations in 2005-2006. The star is most often found in a broad quiescent state between $V \approx 17.4$ and 16.7 mag, but there are frequent bright outbursts to $V \approx 15.2$ mag. Eclipse data are included, and on a few nights the median magnitude corresponds to eclipse (see Figure 6).

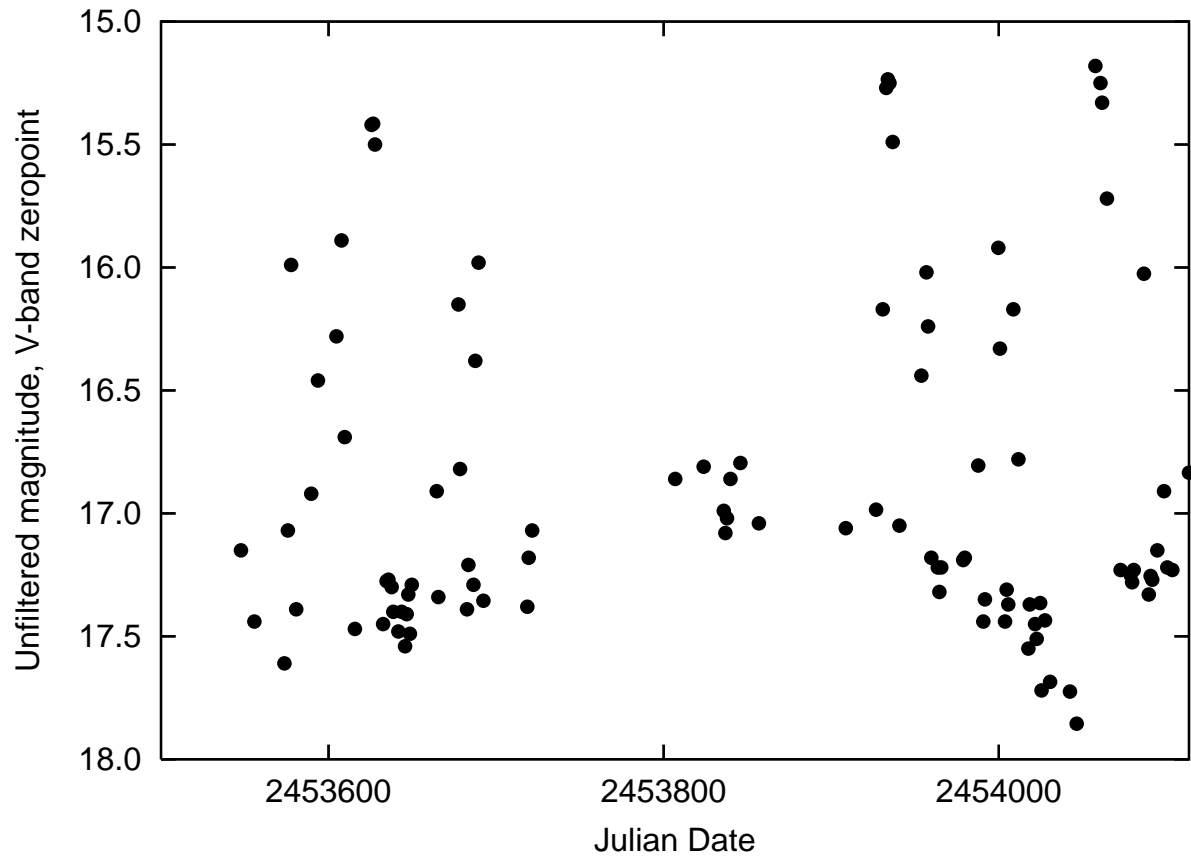


Fig. 6.— Nightly median magnitudes of Lanning 386, showing the irregular outbursts and intermediate states of Lanning 386. The computation of the medians excluded individual magnitudes taken in eclipse.

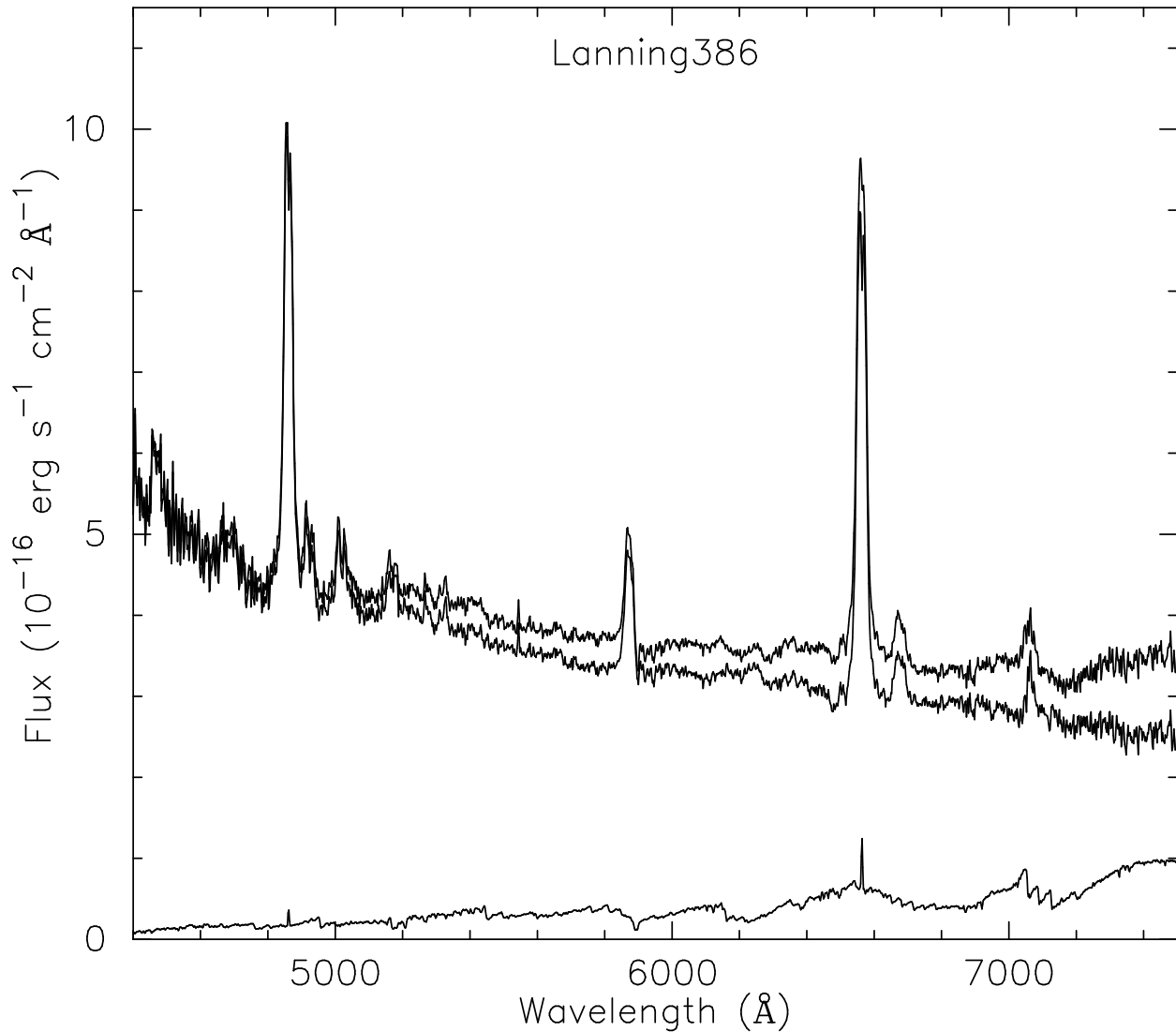


Fig. 7.— *Top trace:* The mean spectrum of Lanning 386 in the low state, from MDM Modspec observations. *Bottom trace:* A spectrum of the M3.5e dwarf Gliese 388, scaled to $f_{\lambda}(6500 \text{ \AA}) = 6 \times 10^{-17} \text{ erg cm}^{-2} \text{ s}^{-1} \text{ \AA}^{-1}$ to approximately match the M-dwarf contribution in Lanning 386. *Middle trace* The difference of the top trace and the bottom trace.

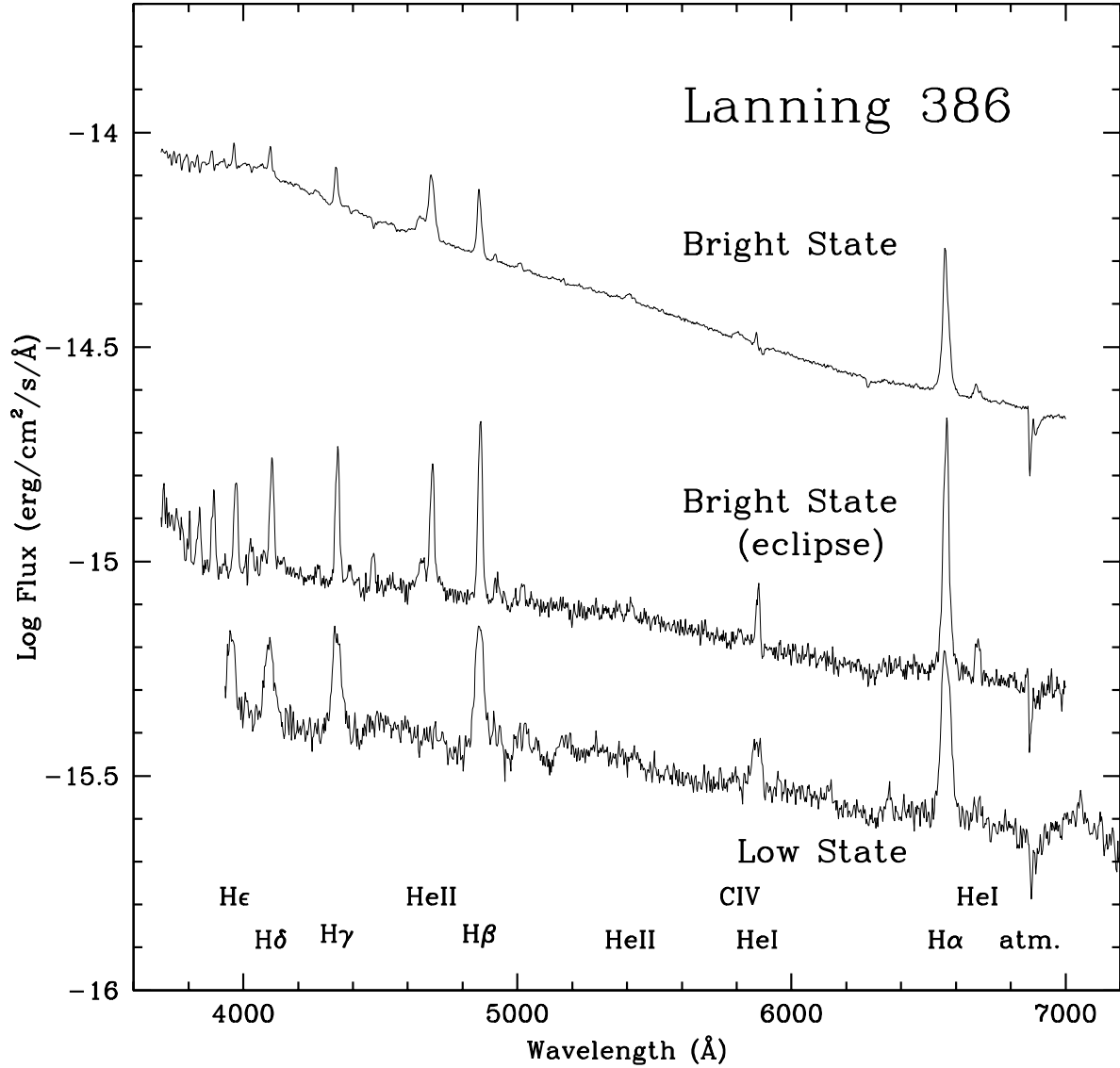


Fig. 8.— *Top two traces:* The average of KPNO spectra taken outside eclipse (top) plotted with the spectrum during eclipse (middle) and an MDM CCDS spectrum taken at quiescence (bottom). The spectrum in the bright state shows a very blue continuum outside of eclipse. In the bright state, Balmer emission lines, emission lines of He I and He II and broad emission from C IV are visible. In quiescence, no high excitation lines are detected.

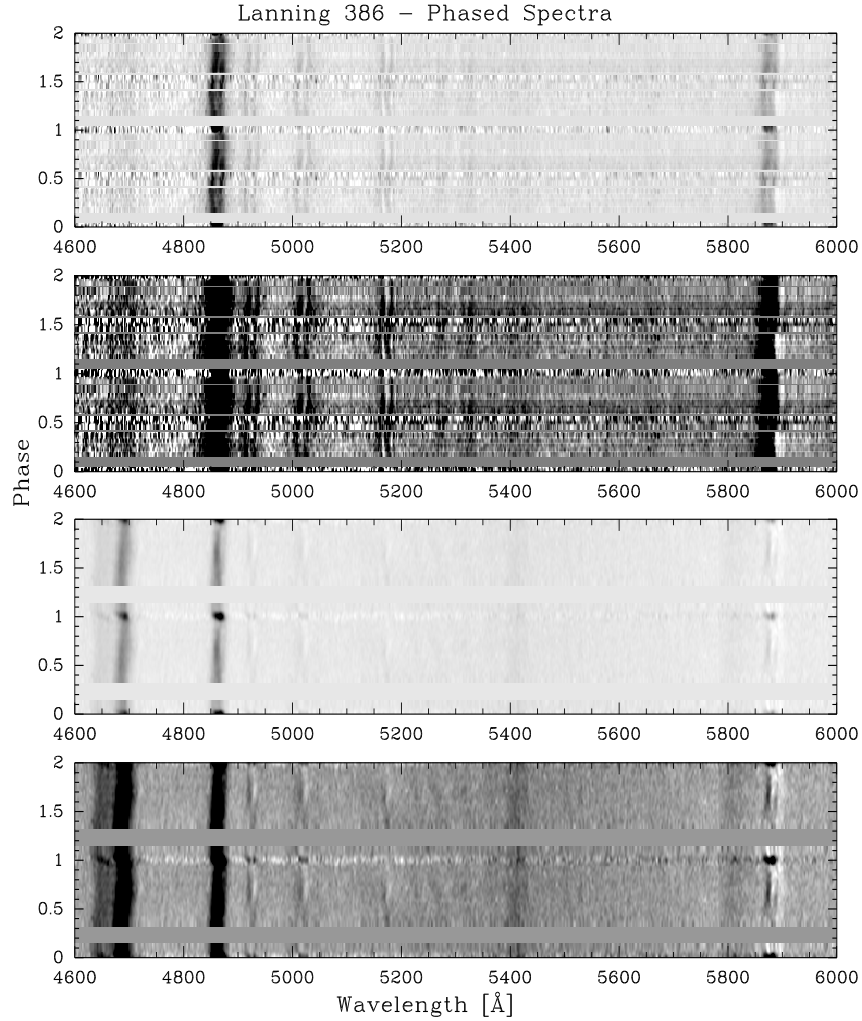


Fig. 9.— Phase-averaged greyscale representations of the MDM Modspec low-state spectra (top two panels) and the KPNO high-state spectra (lower two panels). In the top of each image pair the greyscale is selected to make the details of the strong lines visible, while the lower image is scaled to show the fainter features. The procedure used to create this is described in the text. Blank horizontal bars appear where there are no spectra close enough in phase to include, and other horizontal features are mostly from inadequate phase coverage, except for the eclipse, which is the low signal-to-noise stripe at phase 1. The apparent increase of the emission strength through eclipse is an artifact of the normalization used.

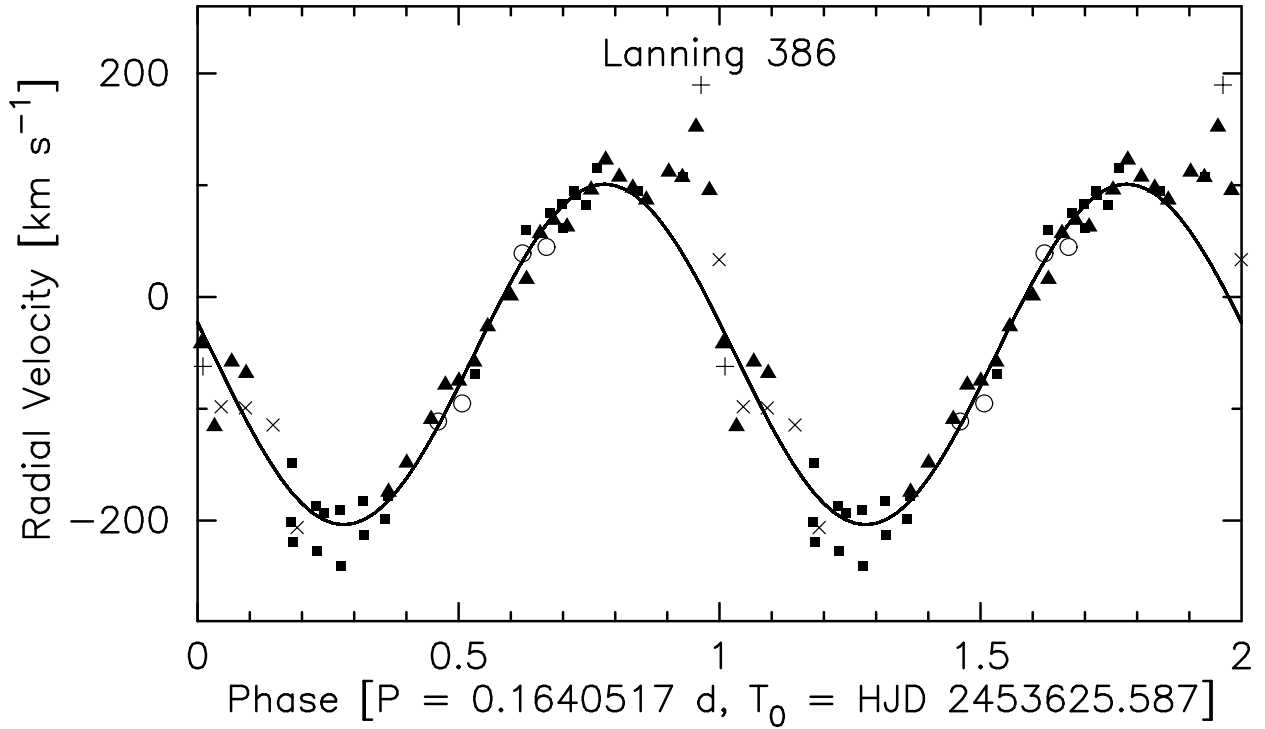


Fig. 10.— Radial velocities of $\text{H}\alpha$ from the MDM Modpsec and KPNO 4m, folded using the eclipse ephemeris. The solid triangles are the KPNO high-state data; the X-crosses are from 2005 Sep high-state spectra; the remainder were all taken in the low state, and the symbols denote different observing runs as follows: plus-signs = 2005 July; solid squares = 2006 Aug/Sep; open circles = 2007 Mar/Apr. All the velocities are re-plotted for a second cycle to preserve continuity. Note the prominent rotational disturbance around the eclipse phase.